Mixing zone growth rate in a direct numerical simulation and wavelet analysis of Rayleigh-Taylor multimode instability development

V.Rozanov[1], R.Stepanov[1], A.Nuzhny[1], R.Yakhin[1], M.Anuchin[2], N. Proncheva[4], N.Zmitrenko[4], Yu.Yanilkin[3], V.Tishkin[4]

[1] *P.N.Lebedev Physical Institute of the RAS, Moscow, Russia*
rozanov@sci.lebedev.ru

[2] *RFNC –VNIITF, Snezhinsk, Russia*
m.g.anuchin@vniitf.ru

[3] *RFNC–VNIIEF, Sarov, Russia*
yan.md08@vniief.ru

[4] *Institute of Mathematical Modeling of the RAS, Moscow, Russia*
zmitrenko@imamod.ru

Abstract

More than 250 numerical simulations (DNS) of Rayleigh-Taylor (RT) and Richtmyer-Meshkov (RM) instability were carried out. The geometry of the problems was two- and three-dimensional (10% of the number of all the simulations). The initial conditions included different initial amplitudes and mode composition of the perturbations, different Atwood numbers, and different statistical realizations of the similar initial conditions basing on a random selection of the perturbation phases involved in the problem. On the basis of this database there was developed an analytical model of the mixing zone taking into account the data on the initial conditions of the perturbations. One more application of the database is connected with the wavelet analysis of the density distribution. In this approach the density distribution of the studied version of instability development for the chosen moment of time is presented as a point in a multidimensional space of wavelet coefficients, and the whole studied version corresponds to the trajectory in the given space. The behavior of the trajectories is studied with the help of the 2D Kohonen maps. This allows one to create a program, which predicts the mixing zone characteristics basing on the initial data.

The given work is the account of the invited paper reported at the 9th International Seminar on the Physics of Compressible Turbulent Mixing, Cambridge, England, 19-23 July, 2004.

The work was supported by the ISTC Project #1481.

Introduction

For many tasks connected with the instability development it is important to predict a development of mixing basing on the information about initial conditions. Within the framework of such an approach, the problem becomes topical, for example, for the tasks of the target compression stability in the ICF. We have performed about 250 DNS calculations of RT and RM instability and mixing for different amplitudes and mode spectra of the initial perturbations, and different Atwood numbers. For the perturbations of the same type, the simulations were made at a different random selection of the perturbation phases. The geometry of the task was two- and three-dimensional, 2D and 3D (about 10%). The simulations resulted allowed us to obtain the functions *f(x,z,t)* for 2D problems, and the functions *f(x,y,z,t)* for 3D problems (the density fields, the components of the rate, kinetic energy and enstrophy, the size of the mixing zone, the mass of the mixed matter). The simulations were performed with the help of the numerical codes NUT, MAX, and EGAK [2-6], and various test calculations showed that those codes produced similar results. As shown earlier, the simulations with the NUT code reproduced satisfactorily the results from the shock-tube experiments by S.Zaitsev on the development of the RM instabilities [1]. The MAX and EGAK codes were also experimentally confirmed. The data concerning the formulation of the problem are illustrated in Fig. 1a and b, and the comparison of the NUT and EGAK numerical simulation results is presented in Fig.1c.

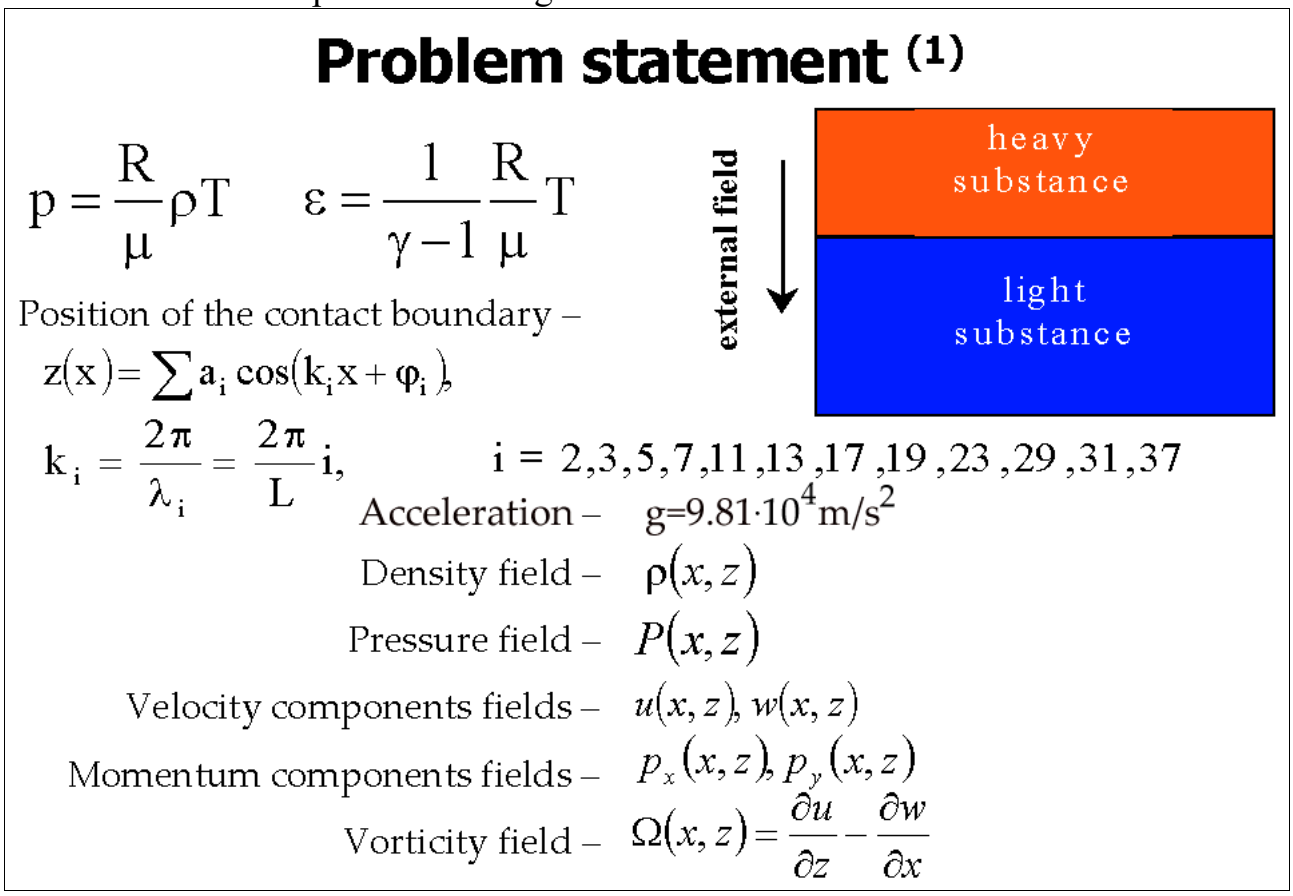

Fig.1a. Formulation of the problem.

Problem statement (2)

Instabilities: RT, RM, limited time of development

Dimension: 2D and 3D

Amplitudes: $a_k^o = a_o(k)$

$$\begin{cases} 1.\ a_k^o k = \text{const} \Rightarrow a_k^o = \dfrac{\text{const}}{k} \\ 2.\ a_k^o = \text{const} \end{cases}$$

Modes: N_{max}=6,8,10,12; i=2,3,5,7,11,13,17,19,23,29,31,37

Phases: random choice on the interval 0 —2π

Attwood number: Ar/Xe A=0.532 ; He/Xe A=0.941

Total number of simulations: 250

Physic values: the kinetic energy: $E_k = \int_{Z_{min}}^{Z_{max}} \int_{X_{min}}^{X_{max}} \rho \frac{u^2 + w^2}{2} dxdz$

$\int_{Z_{min}}^{Z_{max}} \int_{X_{min}}^{X_{max}} \rho w\, dxdz$: z-component of a momentum

the width of the mixing zone: $L = Z_2 - Z_1$

$\int_{Z_{min}}^{Z_{max}} \int_{X_{min}}^{X_{max}} C\rho\, dxdz$: the mass of heavy fluids involved into mixing

the enstrophy : $H = \frac{1}{2} \int_{Z_{min}}^{Z_{max}} \int_{X_{min}}^{X_{max}} \Omega^2(x,z,t)\, dxdz$

Fig.1b. Formulation of the problem.

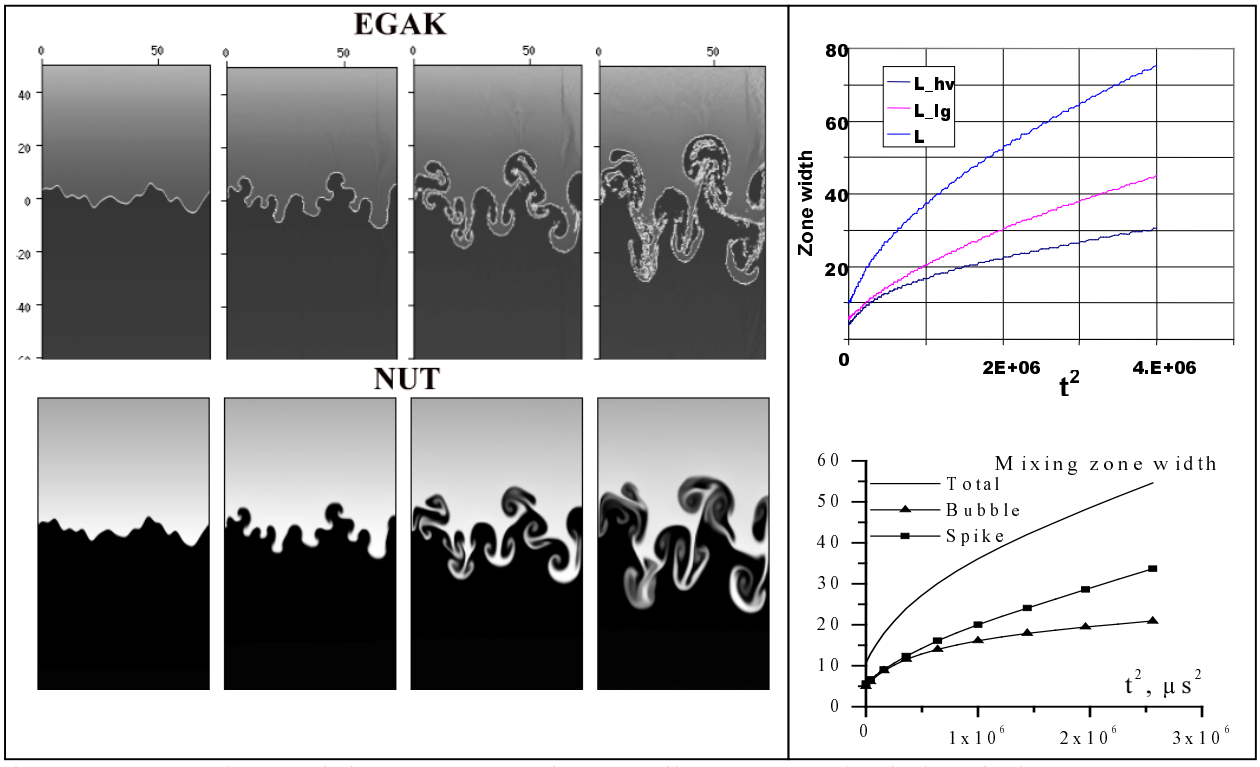

Fig.1c. Comparison of the EGAK and NUT direct numerical simulations (DNS)

1. The results of numerical simulations

The numerical results give an answer to the question about the influence of the perturbation initial amplitude and the presence of high harmonics in the spectrum. Only the prime numbers of 2,3,5,7,11,13,17… were used for the harmonics numbers. The simulations with the number of harmonics N=6 contained the mode with n=13 as the maximal harmonic. For the total number of modes, N=12, the highest harmonic was the mode with n=37. The initial amplitudes were determined either by the law a_o=const/k (k=2π/λ) or a_o=const. The second case corresponded to the initial conditions with the overestimated influence of the higher harmonics. The results obtained in a number of simulations, which illustrate those dependencies, are shown in Figs.2-7.

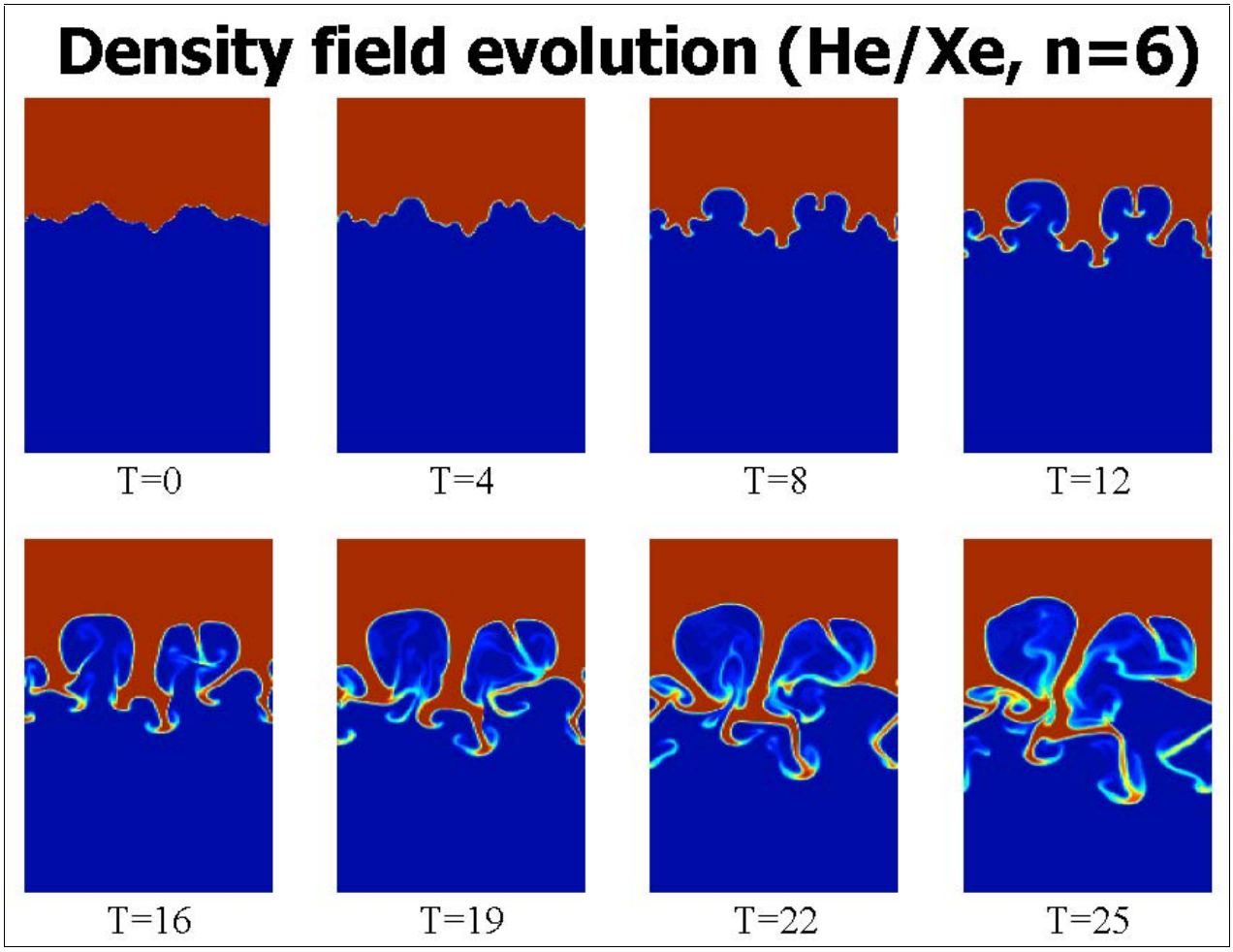

Fig.2. Evolution of the density field, the calculation result.

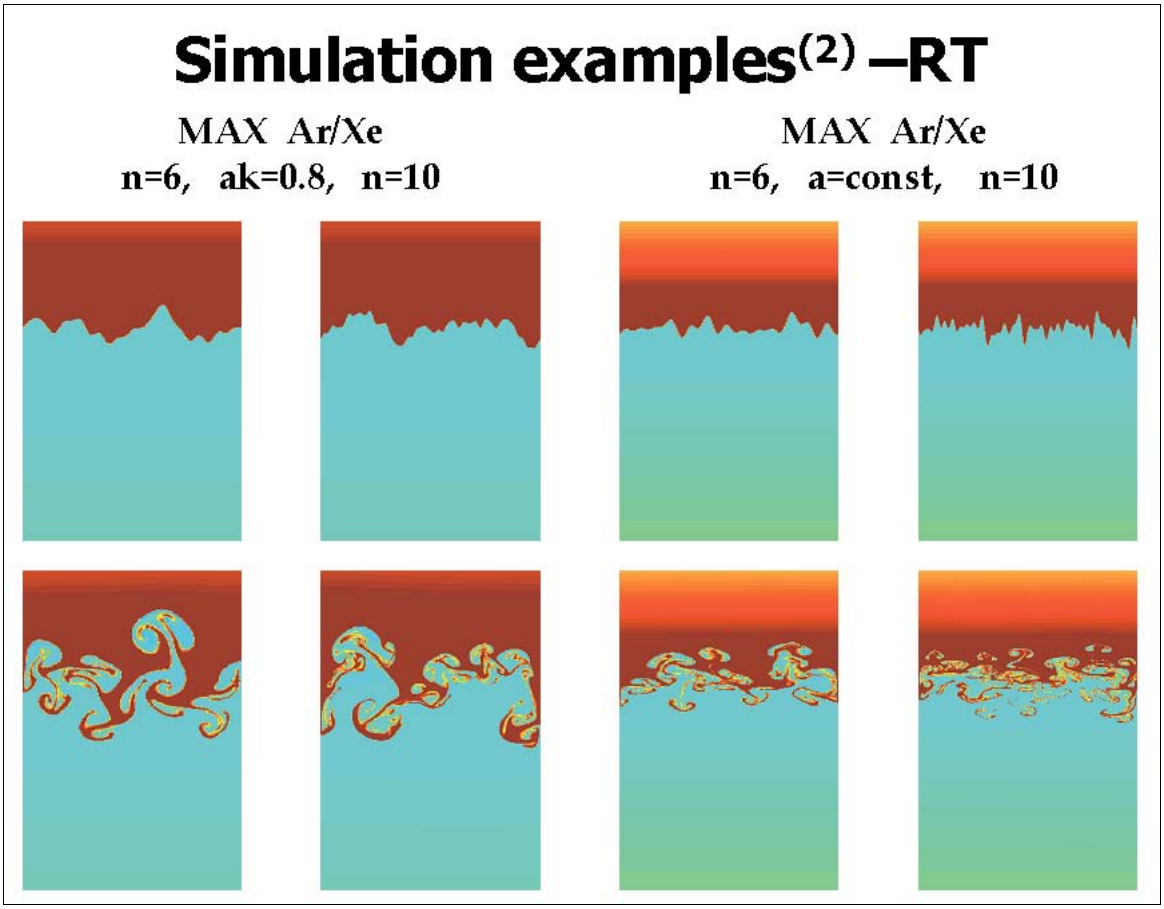

Fig.3. Example of the RT-instability calculation, 2D, A=0.941.

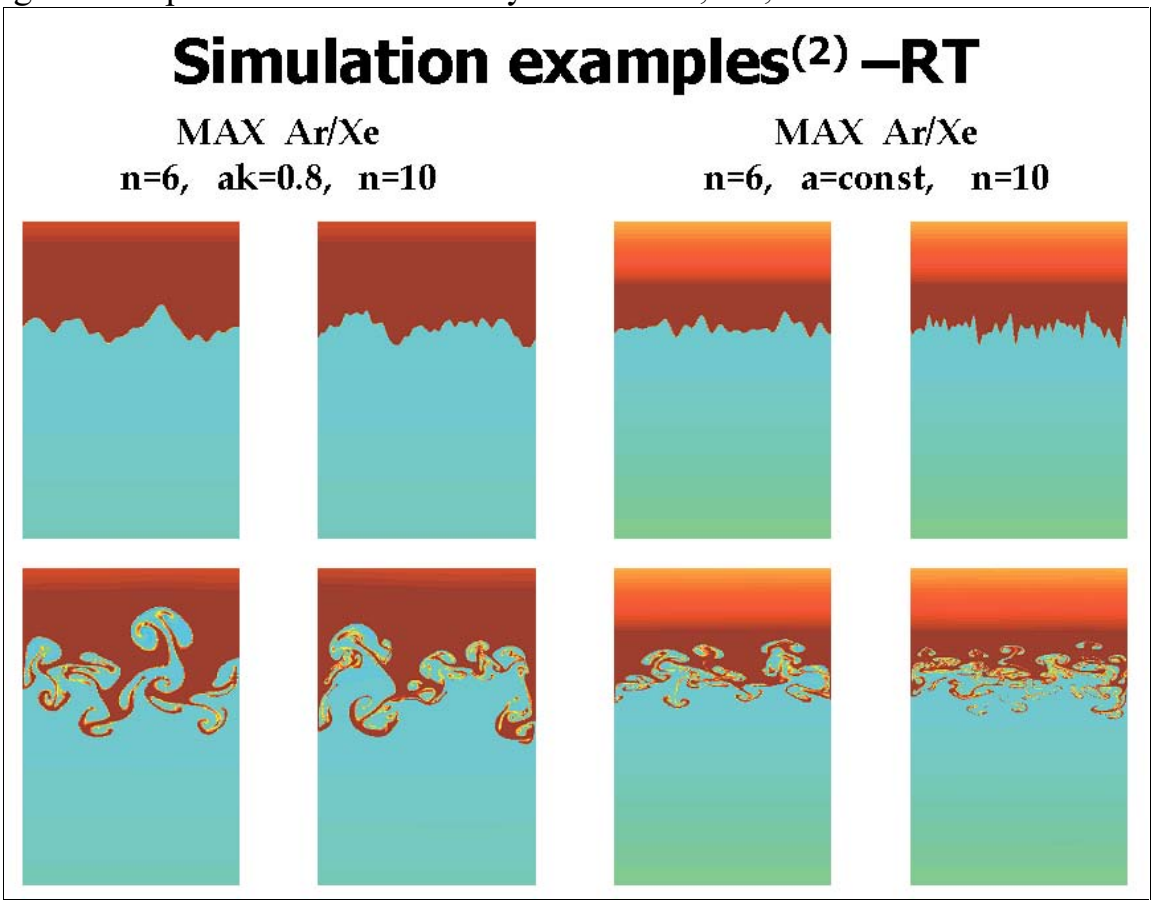

Fig.4. Example of the RT-instability calculation, 2D, A=0.531.

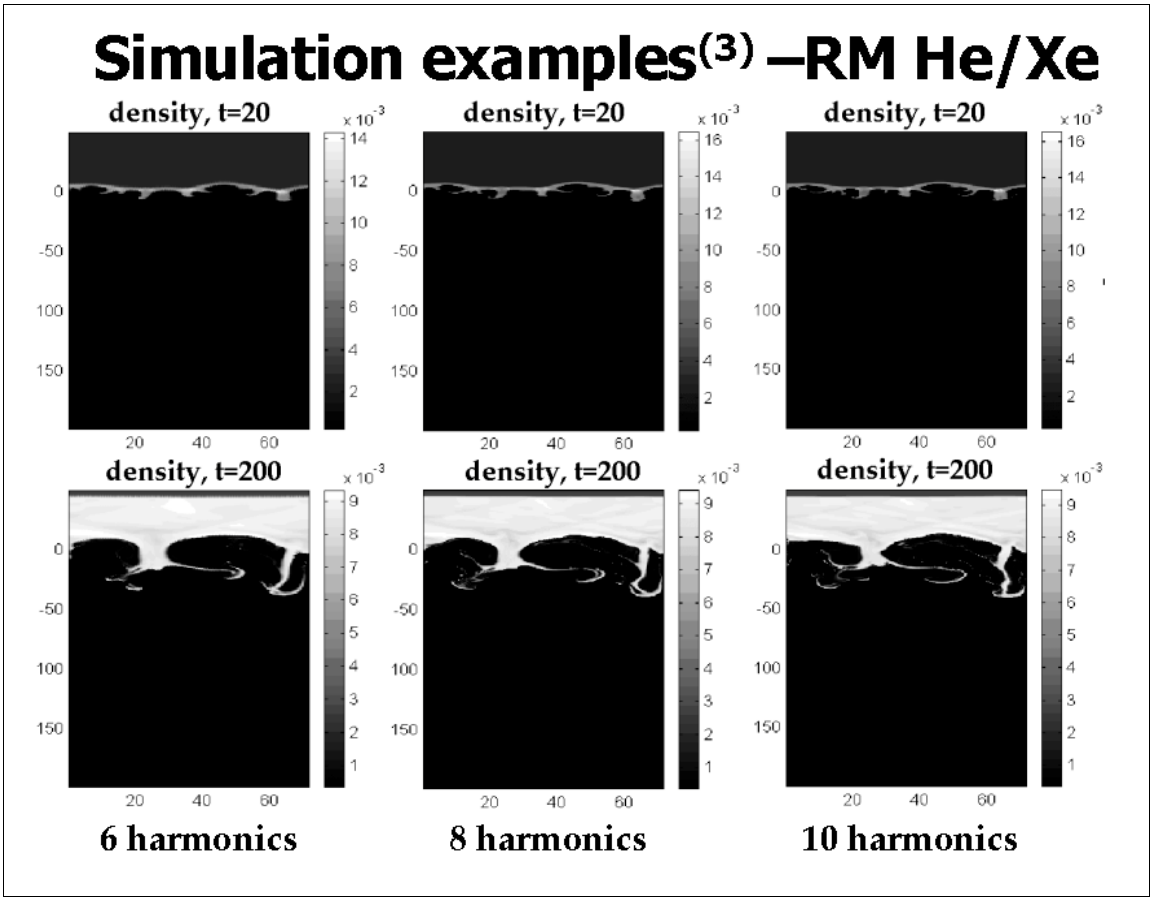

Fig.5. Example of the RM-instability calculation, 2D, A=0.941.

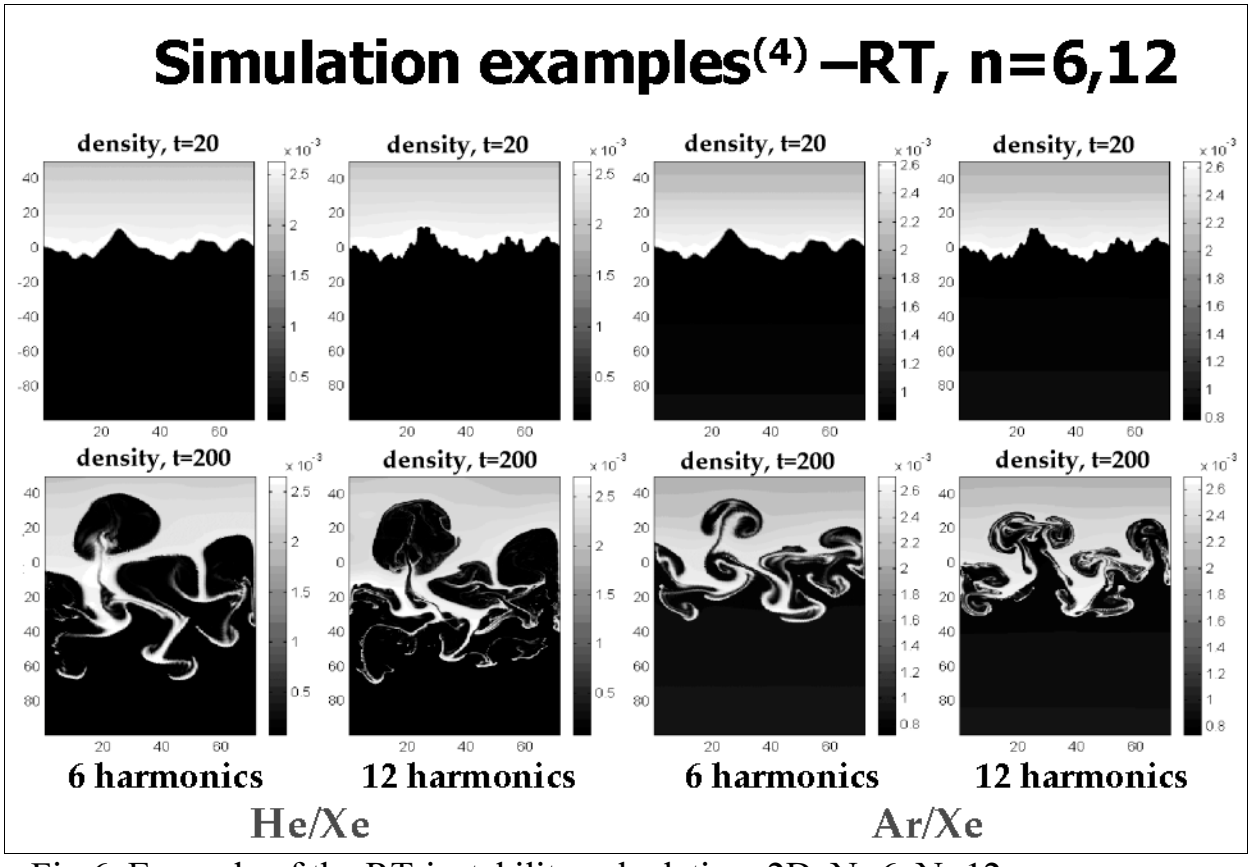

Fig.6. Example of the RT-instability calculation, 2D, N=6, N=12.

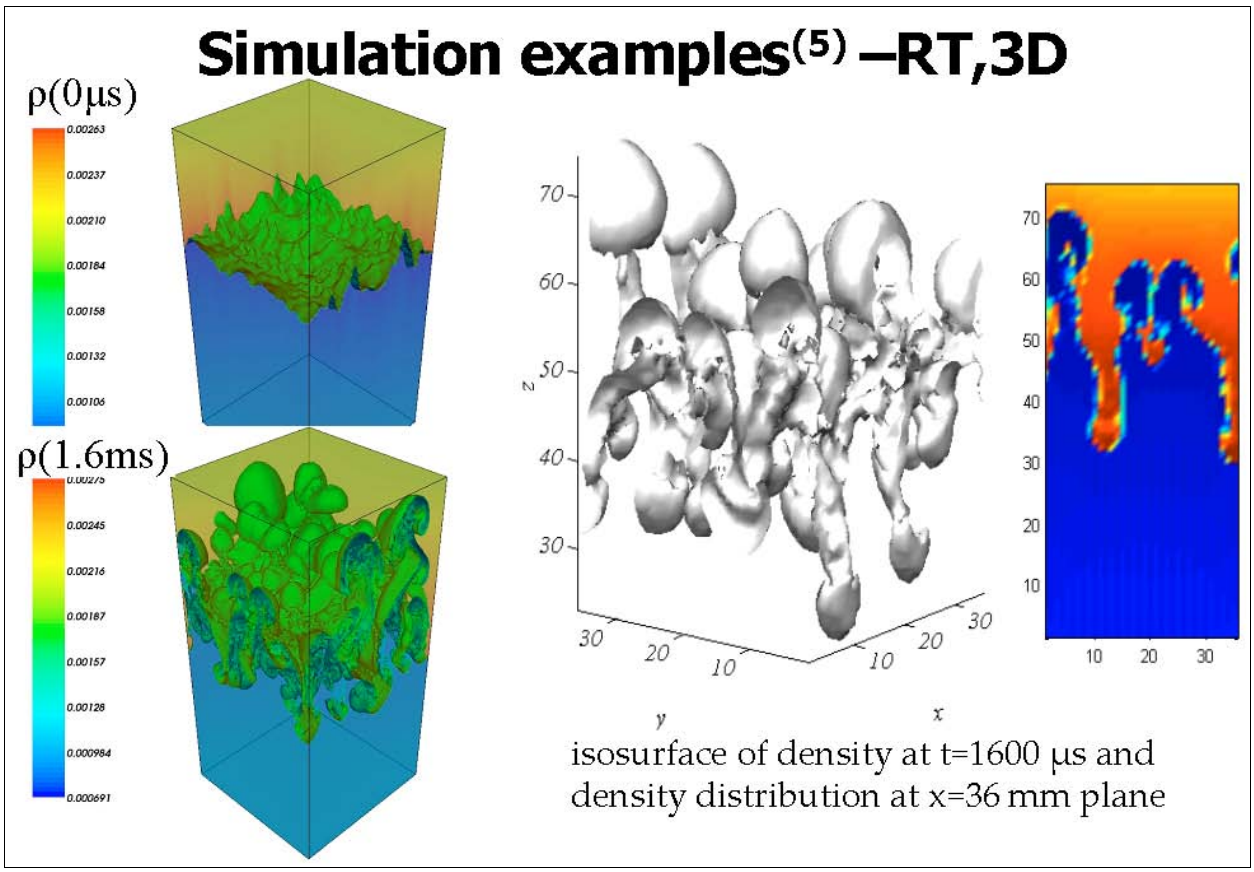

Fig.7a. Example of the RT-instability calculation. Code MAH, 3D, N=6, A=0.531

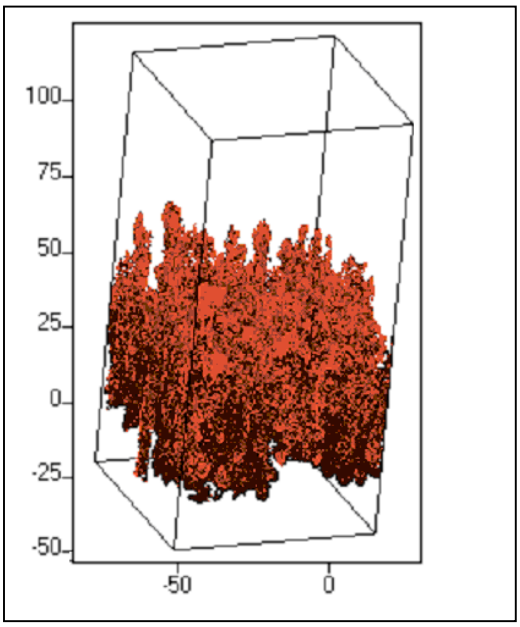

Рис.7b. Example of the RT-instability calculation. Code EGAK, 3D, 1.2μs, N=6, A=0.531

Figure 8 a and b demonstrates the time behavior of some values for 2D and 3D geometry (N=6, A=0.531) under the development of RT instability:

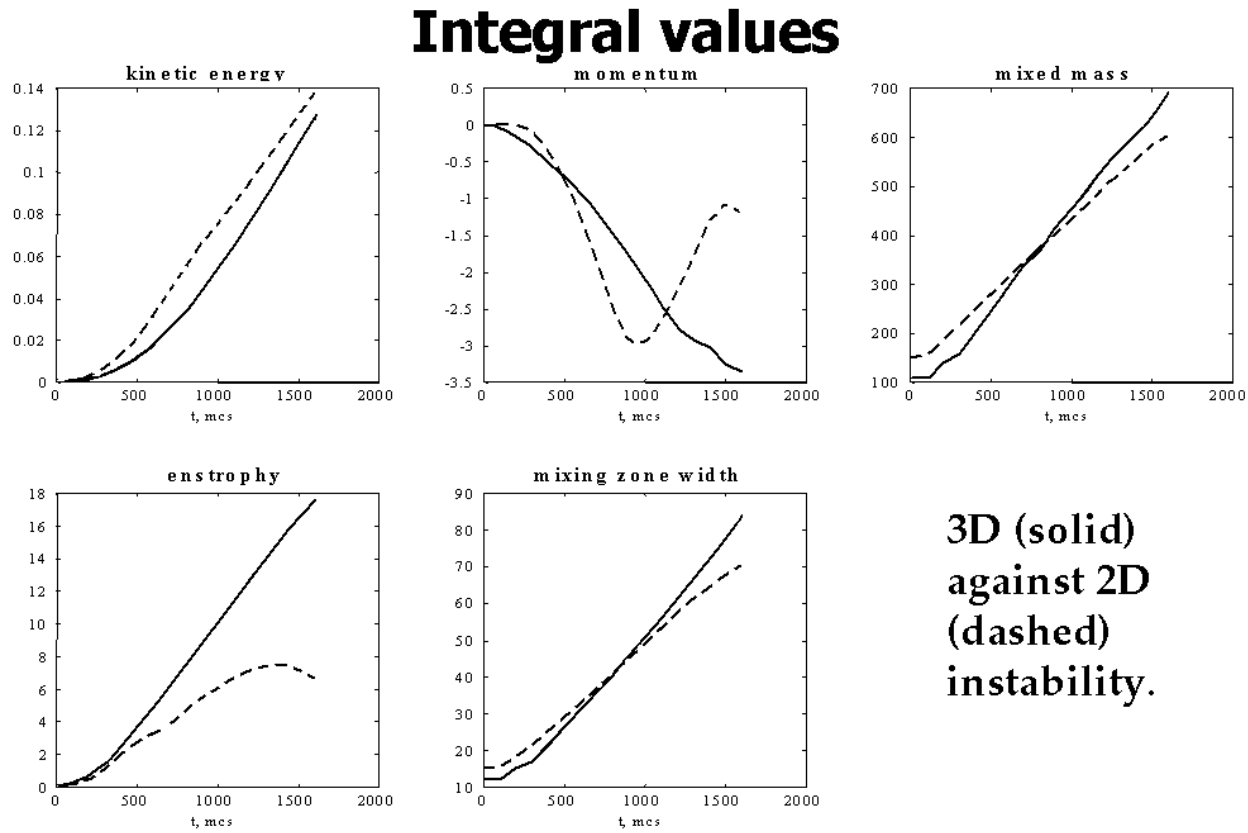

Fig.8a. The mixing zone width and other parameters in the calculations using code MAH for 2D and 3D initial perturbations (N=6, A=0.531)

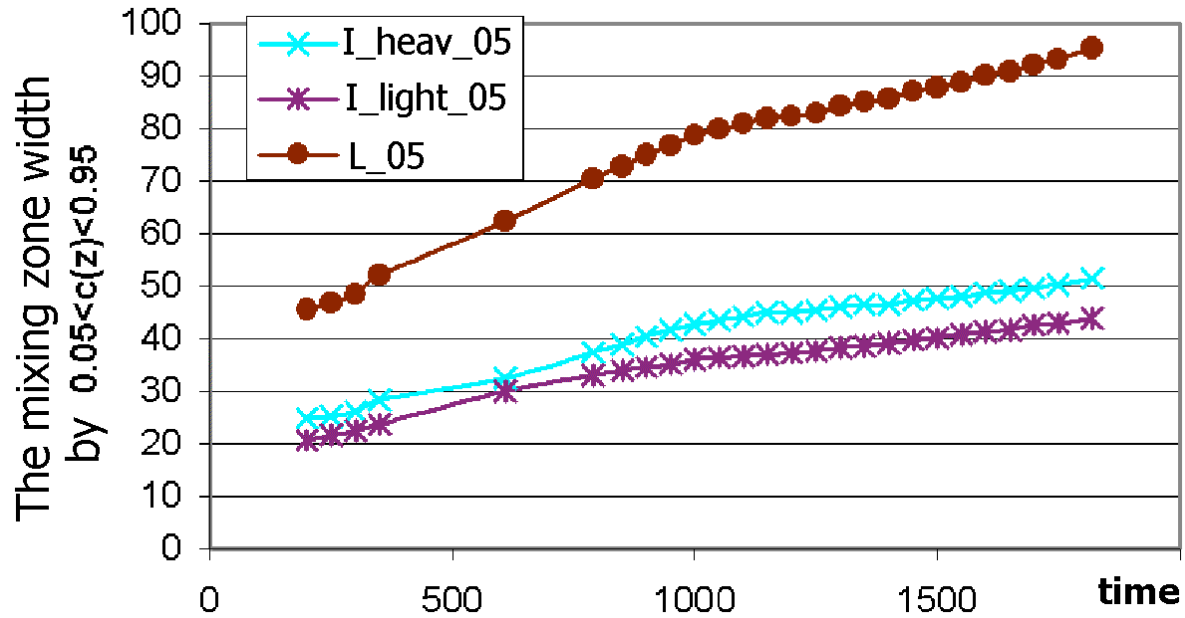

Fig.8b. The mixing zone width in the calculations using code EGAK for 3D initial perturbations (N=6, A=0.531)

The results of this part of the research may be summarized as follows:

- Basing on the DNS simulations, a vast database was produced on the development of instabilities and mixing of two gases, at constant acceleration, for different regimes having different types of instabilities (RT and RM), geometry (2D and 3D), and Atwood numbers (0.941 и 0.532); different

numbers of the modes taken into account, and, correspondingly, the maximum number of the shortest mode (n=13 and n=37), different initial amplitudes, and the dependence of the amplitude on the mode number (a=const/k and a=const);
- At the studied stage, the mixing zone width essentially depends on the amplitude of the initial perturbations and changes with time in accordance with the law close to the linear one;
- The mixing zone width weakly depends on the contribution of the higher modes (it slightly decreases if the higher modes are taken into account);
- The mixing zone widths of 2D and 3D cases turn out to be close at close initial conditions.

2. The mixing zone growth rate

A development of multi-mode perturbations does not provide conditions for deriving simple analytical relations, which could determine the width of the mixing zone in respect to initial conditions. The DNS results may yield such a formula at the assumption of correct asymptotics at the beginning of the process and at its later stage. The zone increases with time by square law at the beginning of the process in the presence of higher modes. This follows from evolutionary model of the instability development [6]. At a later stage, the zone growth rate tends to the constant limit value, which is determined by the floating-up rate of a light liquid bubble (ball). A size of the ball is defined by a lower harmonic, which has been developed by that moment (the Layzer model [7]). The "i"-th harmonic makes the mixing zone larger by the value:

$$Li(t) = L_{oi} + \frac{\lambda_i f}{\alpha_{eff}}\left(\sqrt{1+\frac{(\alpha_{eff}\gamma_i t)^2}{2\pi f}} - 1\right)$$

Here $\gamma_i^2 = \frac{2\pi}{\lambda_i} gA$, $A = \frac{\rho_2 - \rho_1}{\rho_2 + \rho_1}$, $f = \frac{\upsilon^2(A)}{A}$, $\alpha_{eff} = \frac{\alpha_o \cdot \alpha^*}{\alpha_o + \alpha^*}$, $k_i = \frac{2\pi}{\lambda_i}$, $\alpha_o = k_i a_{oi}$.

According to [6], value α^* determines the amplitude, at which the exponential growth of instabilities decelerates, because a mushroom structure is formed. Normally, $\alpha^*_{2D} = 3 \div 5$ for the 2D problem, and $\alpha^*_{3D} = 10 \div 20$ for the 3D problem. At small t and small $a_o (\alpha_o < \alpha^*)$, we have $\frac{dL_i}{dt} = a_o k_i g A t = a_o \gamma_i^2 t$ or $\ddot{a} = \gamma^2 a$ in accordance with the linear development of instability at initial velocity equal to 0. At large t, we have $\frac{dL_i}{dt} = \upsilon\sqrt{g\lambda_i}$. In the Layzer model [7], the above velocity defines the maximal velocity of the light bubble floating-up, $V_{\lim} = \upsilon\sqrt{g\lambda_i}$, where $\upsilon(A)$ is the coefficient depending on the problem geometry and the Atwood number A: $\upsilon_{3D}(1) = 0.23$. In the equation for $\frac{dL_i}{dt} = \upsilon\sqrt{g\lambda_i}$, the coefficient υ takes into account both the rate of the light bubble floating-up and a higher rate of a heavy jet dropping. Normally, this coefficient achieves the values within 0.75÷1 for 2D problems, and $\upsilon \cong 1.0$-1.3, for

3D problems. The zone width is determined by a contribution of all the harmonics, but their contributions are different and are changing with time. In the case of one harmonic, $L(t)=2a(t)$, where the contribution of the long-wave perturbations may be of $\approx 2a$, while the short-wave perturbations are of less importance. The zone width may be represented in the form:

$$L(t) = \sum_i Li(t) w_i(t), \tag{1}$$

where $w_i(t)$ is the weight coefficient, which defines the contribution of the given harmonic. At the initial moment, $w_i(0)$ is determined by a random phase of the given perturbation:

$$w_i(0) = \cos(k_i x_{\max} + \varphi_i) - \cos(k_i x_{\min} + \varphi_i) \tag{2}$$

and may be of $w_i(0) \cong 2$, in particular. From the latter relation it is seen that the zone width is determined by a maximally "high" position of light liquid and minimally "low" position of heavy liquid. Then $w_i(t)$ is decreased, which corresponds to damage of the given instability mode due to the Kelvin-Helmholtz instability development [7]. The behavior of $w_i(t)$ may be approximated by the dependence:

$$w_i(t) = w_i(0) e^{-(\gamma_{KH})_i \cdot t} \sim e^{-\frac{1}{2} k_i a_i \sqrt{1-A^2}} \sim e^{-\frac{1}{4} k_i a_i^o \sqrt{(\gamma_{RT})t}}.$$

Here:

$$(\gamma_{KH})_i = k_i \nu_i \frac{\sqrt{\rho_1 \rho_2}}{\rho_1 + \rho_2}, \quad \nu_i t = \frac{a_i^0}{2}\left[e^{(\gamma_{RT})_i t} + e^{-(\gamma_{RT})_i t}\right] = a_i^0 \left[1 + \frac{(\gamma_{RT} t)^2}{2}\right]$$

and v_i is the velocity of the heavy liquid jet growth in the "i"th harmonic RT instability.

Values γ_{KH} and γ_{RT} depend on the wave vector $k_i = \frac{2\pi}{\lambda_i} = \frac{2\pi}{L} n_i$ and thereby depend on the "i"-th harmonic's number, which is not always marked in the above formulae. It is seen that a contribution into the zone width of the harmonic with the number n_i decreases the faster the higher the number n_i. If the spectrum of initial perturbations is $k_i a_i^o = \text{const}$, then $w_i(t) \sim e^{-c_1 n_i}$. If the initial perturbations correspond to the law $a_i^0 = \text{const}$, then $w_i(t) \sim e^{-c_2 n_i^2}$. Basing on those assumptions, we have performed calculations of the mixing zone width by using Eq. (1), where the weights $w_i(t)$ were determined in accordance with the above model. In the other variant, the weights $w_i(t)$ were chosen by a better coincidence of $L(t)$ with the DNS results.

It was found that at the later stages the contribution of higher harmonics was not of a zero value, and it is desirable to take it into account. As it turned out, the high-frequency modes make a contribution into the mixing zone width equal to $a_{mix} \cong (3 \div 5)\lambda/2\pi$, for 2 D geometry, and for the 3D geometry the contribution is $a_{mix} \cong (10 \div 20)\lambda/2\pi$ [6]. Both variants give rather close results, which support a validity of the above speculations. Some of the results of comparison of the DNS

zone width data with the $L(x)$ calculations and the behavior of the coefficients ω_i are represented in Figs.9 and 10. It seems possible that one can reproduce, with a good accuracy, the DNS results with the help of the relation of the type of Eq.(1). A more important conclusion is that the long-wave perturbations being developed by that moment give the greatest contribution to the mixing zone width. It is easy to calculate the evolution of the perturbations by means of DNS or estimate them by the analytical models described, for example, in [7], because $(\gamma_{RT})_i t$ achieves smaller values for those perturbations.

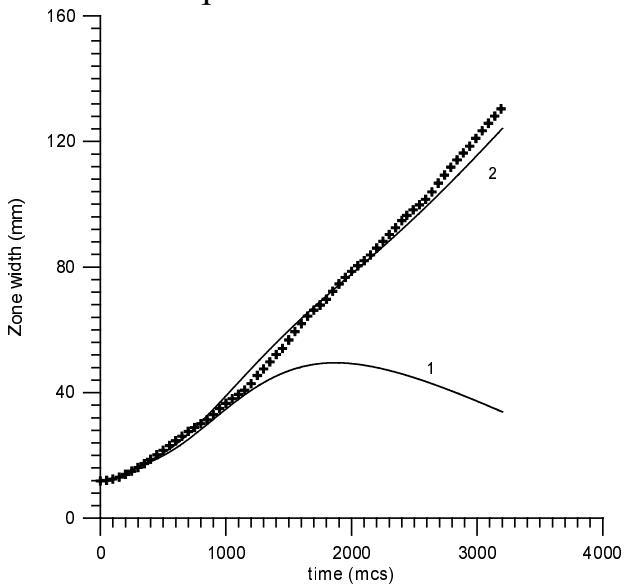

Fig. 9. $L(t)$ dependencies for two variants of $w_i(t)$ coefficients (see Fig.10): "+" corresponds to the DNS results

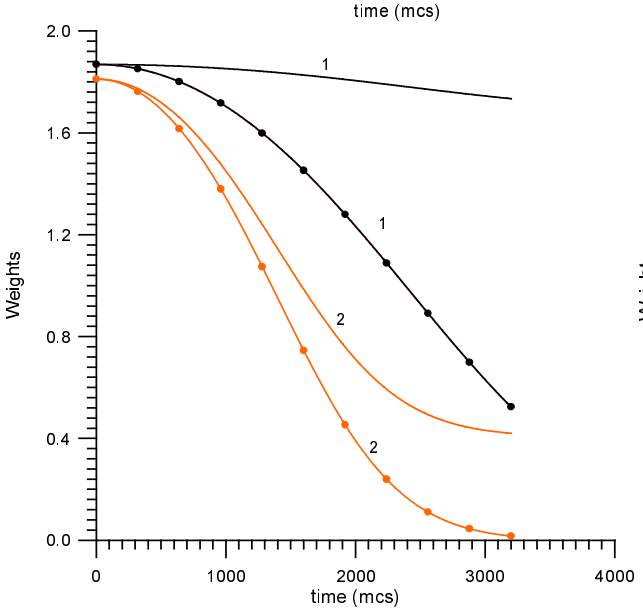

Fig. 10a. The coefficients $w_1(t)$ и $w_2(t)$ evolution for the curves 1 and 2 of Fig.9

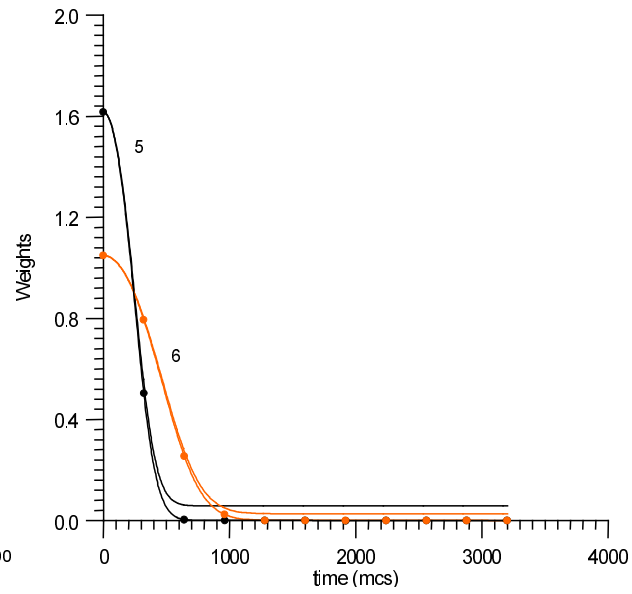

Fig. 10b. The coefficients $w_5(t)$ и $w_6(t)$ evolution for the curves 1 and 2 of Fig.9

For the theory it proved to be important that decreasing of the term $e^{-\gamma_{KH} t} = e^{-\frac{\gamma_i^2 t^2}{l_i^2}}$, where l_i is the fitting parameter, had been time limited. This limitation means that the perturbation occurring after the destruction (achievement of

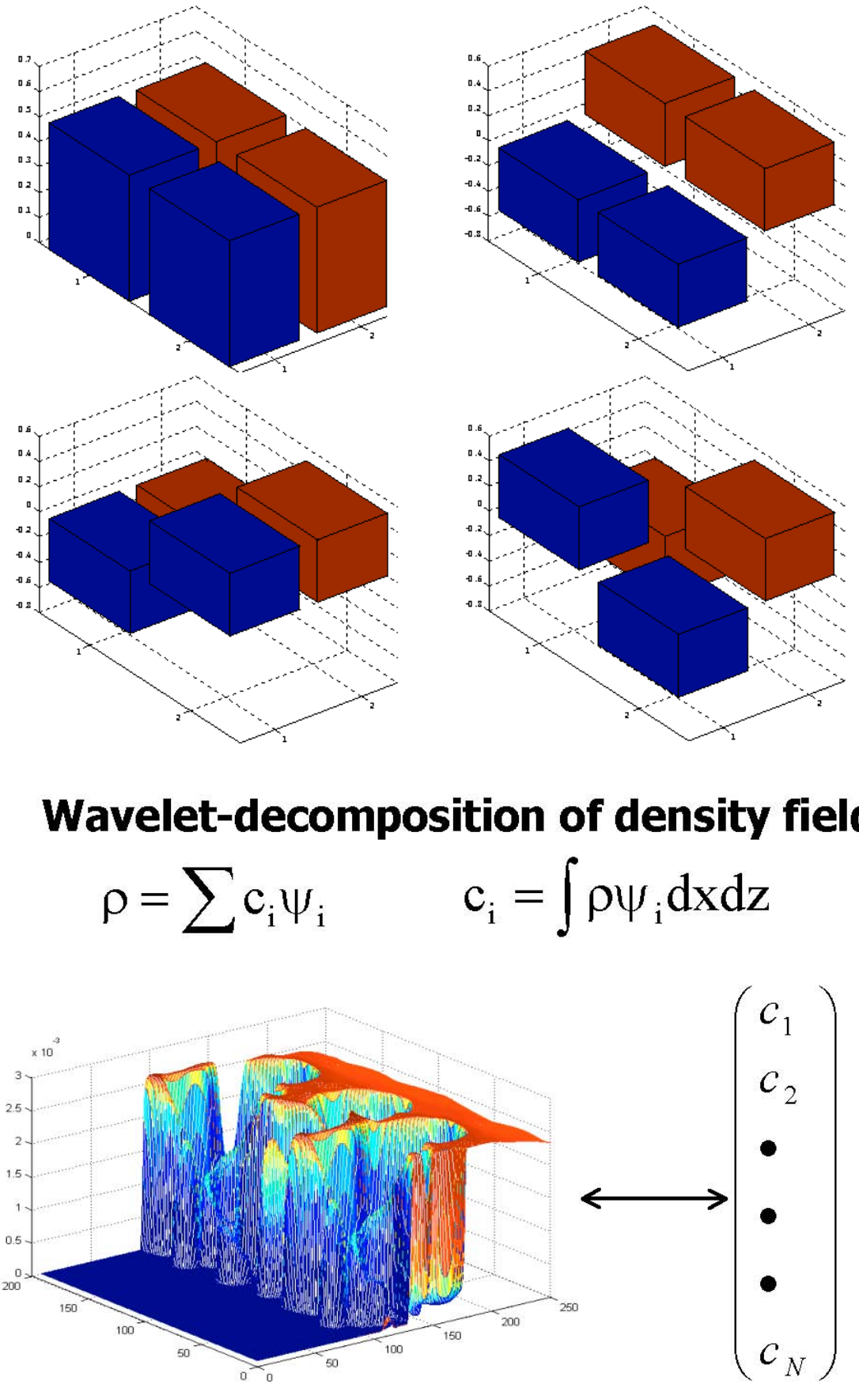

Fig. 11. Wavelet D1 and the density field decomposition

the "critical age") still affects the zone width. Figure 9 illustrates two theoretical curves $L(t)$ as compared to the Rayleigh-Taylor instability calculation (Ar-Xe pair of gases, six harmonics with the constant initial age a_o=0.5). Curve 1 corresponds to the unrestricted decreasing of the weights and curve 2 illustrates turning of the exponential term to the constant value of $0.9/i^2$, where i is the harmonic's number. The behavior of weights is illustrated in Fig.10a (for the first and second harmonics) and in Fig.10b (for the fifth and sixth harmonics). The curves for the unrestricted decreasing of the weights are marked.

3. Wavelet analysis

The DNS results on the RT and RM development at a stage of the mixing layer formation are reported in section 2. The number of the calculations connected with a variety of problems (geometry, type of instability, Atwood number, perturbation spectrum, initial conditions, different statistical realizations, and different codes) also increases because every calculation contains a succession of the results for 10^4-10^5 moments. If one chooses only 40 moments for each calculation then one gets the data base of 250x40~10^4 images containing information about the studied processes.

To analyze the information we have applied the neuro-computer methods, which do not use the a priori data about the studied processes [8,9].

The following scheme has been developed and realized:

1. A distribution of heavy and light liquid density in the x,z - $\rho(x,z,T_i)$ space (a density field) was chosen in each calculation of instability and mixing with definite initial conditions for 26 moments of time (T_0, $T_1 \ldots T_{25}$);
2. The density field was subjected to a wavelet transform, i.e. the wavelet expansion coefficients were found by a standard procedure:

$$\rho(x,z,T_i) = \sum C^{T_i}_{mnm''n'} \psi_{mnm'n'}$$

where

$$C_{mnm'n'} = \iint \rho(x,z,T_i) \psi_{mnm'n'(x,z)}$$

$$\psi_{nmn'm'} = \psi(x_{nm}, z_{n'm'})$$

is the wavelet function, in which the coordinates are subjected to the scaling and shifting transform:

$$x_{nm} = \frac{x - b_{nm}}{a_m}, \quad z_{n'm'} = \frac{z - b_{n'm'}}{a_{m'}}.$$

As a result, the given density field is determined by a set (multitude) of the coefficients $C^{T_i}_{mnm'n'}$.

Because there is a variety of the wavelet transforms, in the described above scheme, we have tested different variants. A procedure was developed for a calculation of the image entropy [10], which determines a "spread" of the calculations from initial state ("the larger the entropy, the less the informative the image"). As it turned out, the best imaging is yielded by the Daubechies1 (D1)

wavelets. In the D1 wavelets, the most "local" description of the object is used. Perhaps this a nonrandom measure because potentiality of the flow leads to "damping" of the information coming from a "far" distance Δr, in accordance with the law: $\sim e^{-k\cdot\Delta r}$, $k=\frac{2\pi}{\lambda}$.

3. In the space of the coefficients $C^{T_i}_{mnm'n'}$, the given moment of any calculation is shown by a point, and the whole calculation corresponds to a trajectory in that space. The space dimensionality is high, it is determined by a size of the smallest cell in a calculation net, where in our case the number of the cells was 130x250. Then the procedures of the space dimensionality reduction were used [11], among which the main component method proves to be the most comprehensive one. The main information was saved, as the dimensionality was decreased down to 200, and even to 40 and 17. "The information is saved" means that one can reproduce initial picture of density by using the wavelet coefficients, without any substantial loss of information. Perhaps in the other problems (for example, determination of the spectral turbulence), it happens to be inefficient to neglect high-frequency components and reduce dimensionality of space.
4. It is convenient to represent the processes (the instability calculation results) on a two-dimensional Kohonen map [13], whose coordinates prove to be close to the primary and second main components (PMC and SMC).
5. It is possible to build a program block, which can predict the mixing zone parameters on a basis of initial data. The trajectories that are outgoing, at first, from one region (cluster) on the Kohonen map, remain close at the later stages.
6. Figures 11-17 illustrate some of the results. Figure 11 demonstrates a D1 wavelet structure and a scheme of the density field expansion over the wavelet functions. Figure 12 illustrates the examples of reproduction of the density field for different numbers of components. Figures 13-15 demonstrate the results of the Kohonen map utilization in the D1 imaging.

In Fig.13 the map is arranged so that, from top to bottom, the primary main component (PMC) is increased, and from right to left, the second one (SMC) is. The basic tendency of the calculations is the following. As the time of mixing and the mixing zone width grow, the value of the PMC monotonously increases. To the start of the process there corresponds a certain value of the SMC, and as time elapses that value of the SMC remains approximately the same. Figure 14 illustrates final states of the calculations, whose trajectories are plotted in the left, middle, and right-hand parts of the Kohonen map, i.e. at different values of SMC. One can observe similar structures of the computer-chosen pairs. For definiteness sake, we shall say that those calculations have been made by the NUT code. They represent a development of 6-mode perturbations of a pair of Xe/He gases at $a_0\kappa$=0.5 and different randomly chosen initial phases of the perturbations. Figure 15 illustrates the Kohonen map in the D1 presentation, which is built by the calculations of five kinds:

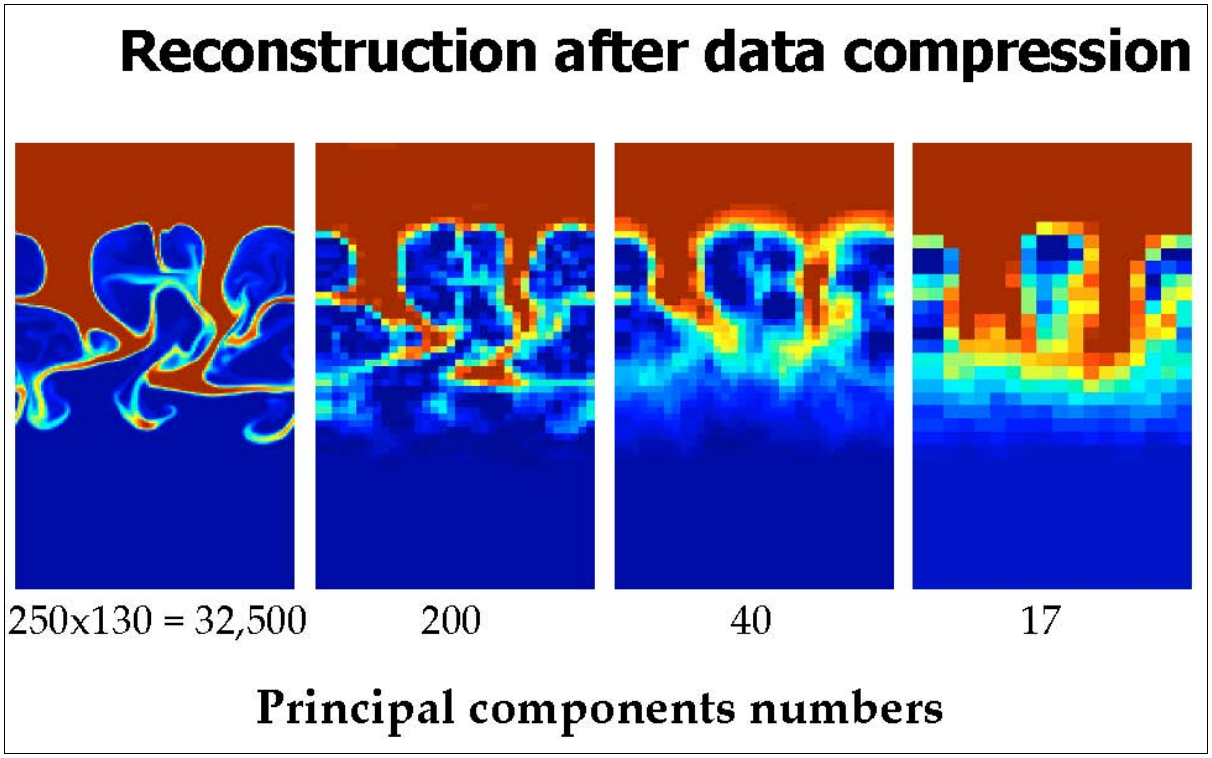

Fig.12. The density distribution field reconstruction for different numbers of kept main components

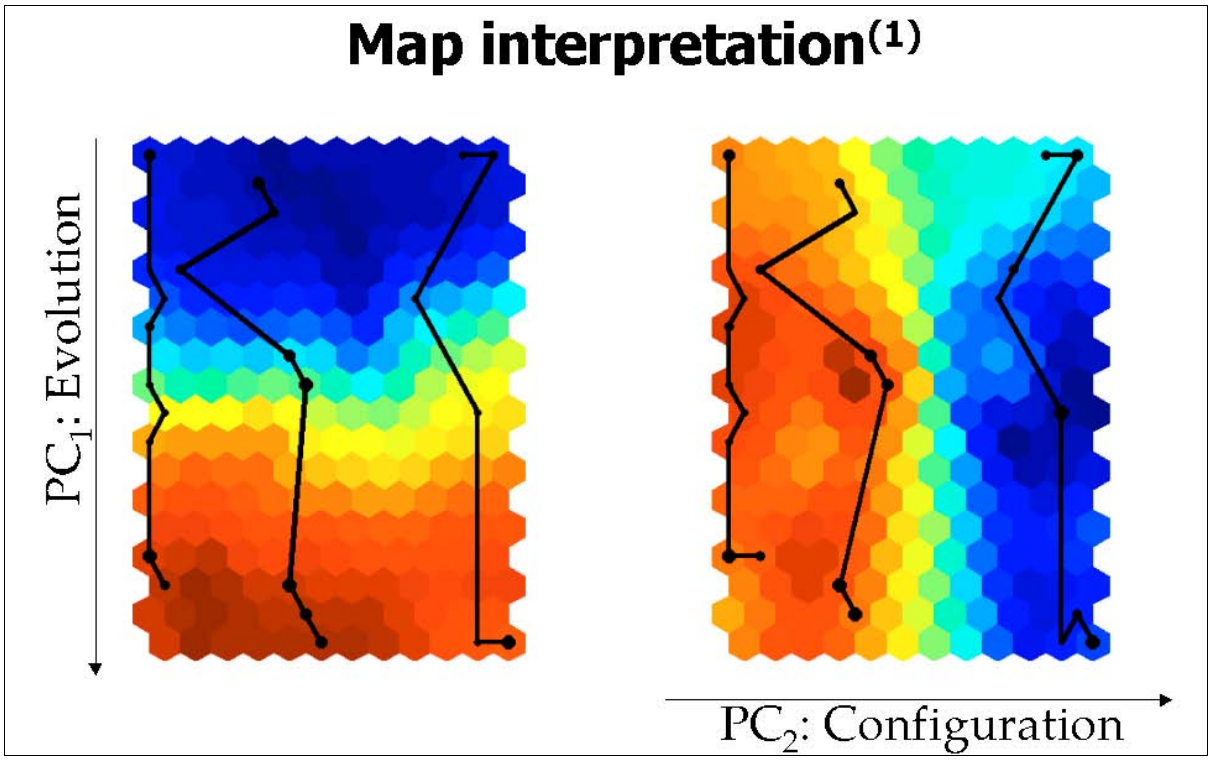

Fig.13. The Kohonen map interpretation

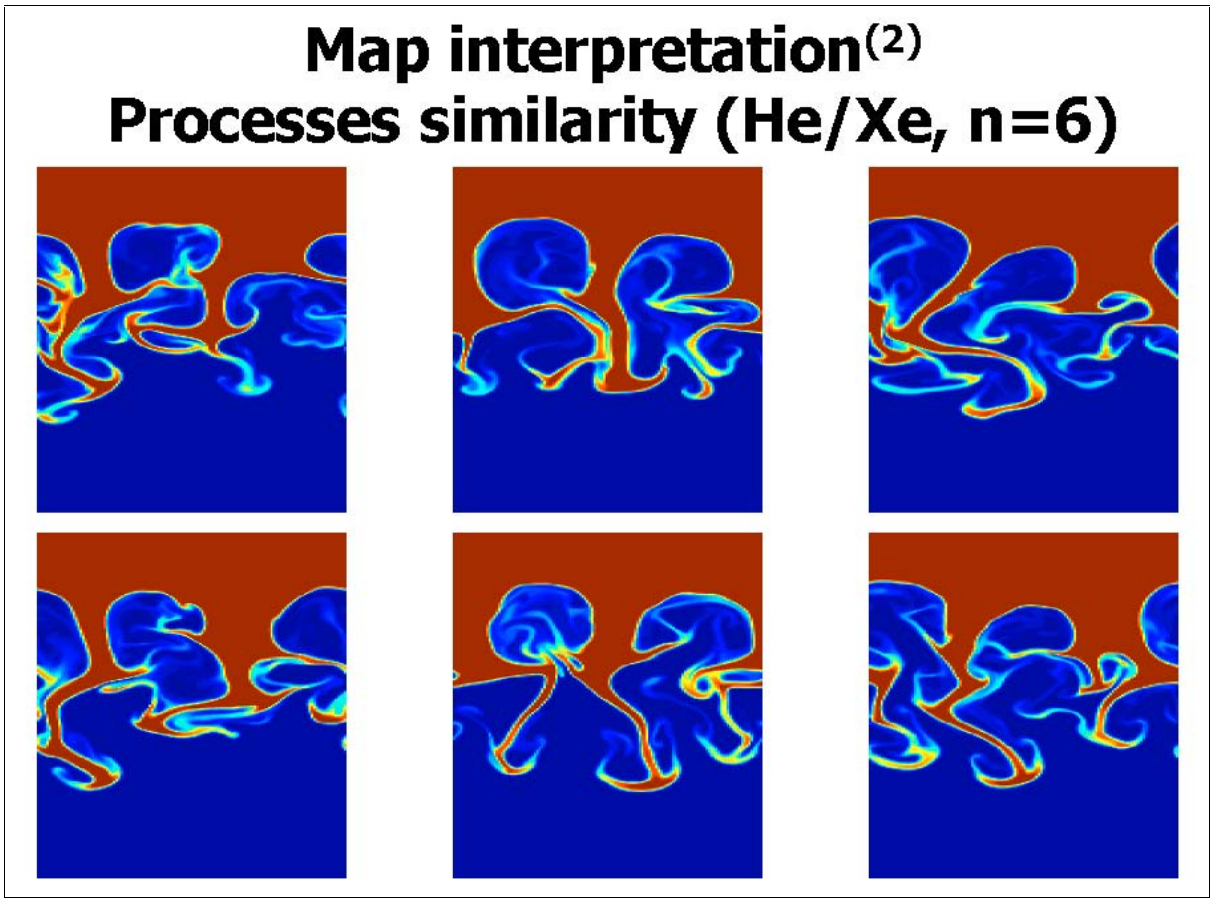

Fig.14. Kohonen map – processes similarity

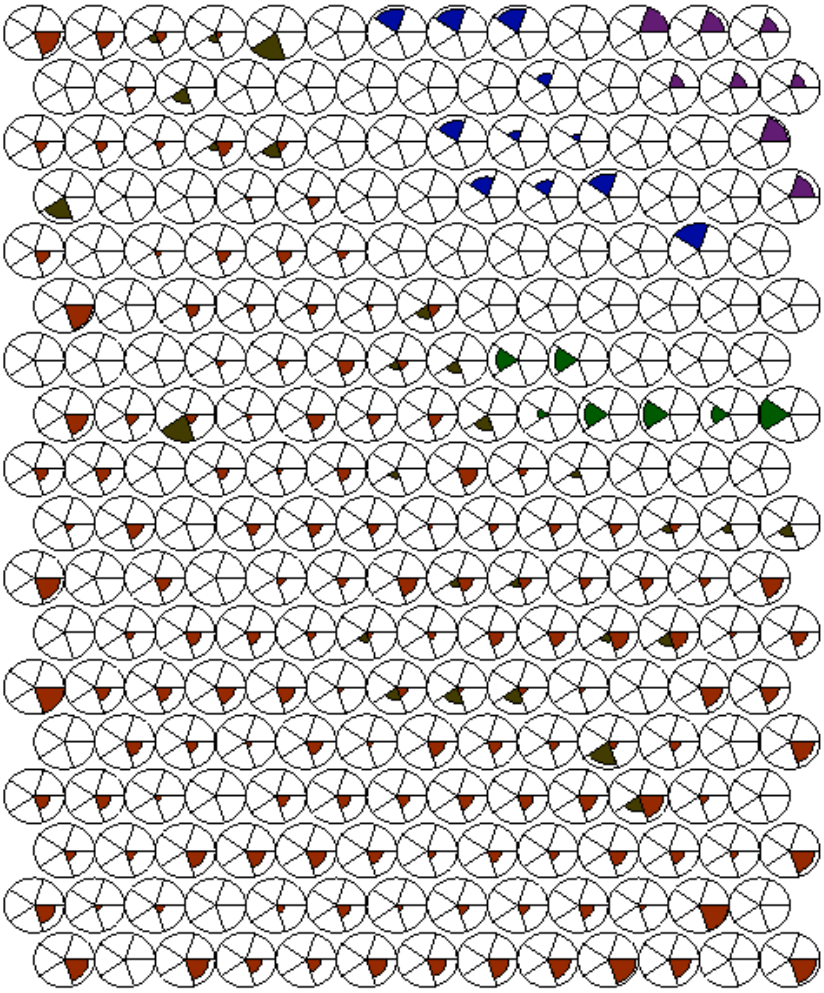

Fig. 15. Kohonen map in D1 representation. Each cell contains 5 sectors for results of 5 calculations:

1. The NUT program: the initial perturbations decrease by the law $a_o\kappa$ =0.5, and the calculations have been performed for the pair of gases He/Xe at A=0.941.
2. The MAX program: $a_o\kappa$ =0.8, He/Xe, A=0.941.
3. The MAX program: a_o=const, He/Xe, A=0.941.
4. The MAX program: $a_o\kappa$=0.8, Ar/Xe, A=0.532.
5. The MAX program: $a_o\kappa$=const, Ar/Xe, A=0.532.

Each cell on a map (a cluster) contains information about each type of the calculations in the form of a circular histogram. Sectors in the histograms are numbered clockwise in the order of 1,2,3,4,5 starting from a four o'clock sector. Filling of the histogram sector is proportional to the number of the calculations of the given type in the given cluster. A comparison of the calculations #1 and 2 (the NUT and MAX codes) shows that they lie in on one site of the map. This suggests that the results obtained by different codes are identical. Actually, as soon as the test calculations had been made we obtained that the used codes produced the identical results. A comparison of the calculations #1,2 and #3 ($a_o\kappa$=const and a_o=const) shows that the calculations #3 occupy a specific part of the map, and they are isolated from other types of the calculations in the space of wavelet images. That property could be used to recognize the processes with higher harmonics. The calculations #4 and 5 (A=0.532, $a_o\kappa$=const, and a_o=const) occupy their own part of the map, which is different from A=0.941, and the cases with $a_o\kappa$=const and a_o=const are separated from each other as well. The calculations with different A (0.941 and 0.532) are separated by a blank on the map (no calculations). It would have been of interest to clarify whether that part might be filled with the calculations (processes) with $0.532<A<0.941$ corresponding to the pairs of gases with another ratio of density (different from Ar/Xe or He/Xe).

As seen from the selected calculations it is possible to compare different mathematical codes on a basis of calculations of the same type, to note the influence of the Atwood number, and to evaluate an increased contribution of high-frequency harmonics in the problems with a_o=const.

Especially interesting is the question about a physical interpretation of the main components. A direct interpretation of the main components proves to be rather difficult due to a high dimensionality of the wavelet space. However, it is possible to perform such interpretation by means of deriving special functions. A convolution of such functions with density distribution for the given moment T_j. $\rho(x,z,T_j)= \rho_j(x,z)$ yields a value of the main component (of the first one, second, and so on), and they may be called the filter functions F_i. Value "*i*" of the main component is obtained by means of those functions starting from the moment "*j*" PC_i^j in accordance with the formula:

$$(PC)_i^j = \rho_j F_i - \overline{c}_k U_{ki} = \int \rho_j(x,z) F_i(x,z) dxdz - \sum_k C_k U_{ki} ,$$

where C_κ are the wavelet expansion coefficients, $C_\kappa=\rho\psi_\kappa$. For the given wavelet ψ_κ, their number is equal to the number of separate pictures of density distribution that are analyzed with account of different types of the calculations and moments (let the number of such pictures be D). Those coefficients will be distinguished by the index α - C_k^α, $1 <\alpha<D$. By using index α we shall determine average value of the coefficient $\overline{c}_k$ and the dispersion of the coefficients Σ_{ij}:

$$\overline{c}_k = \frac{1}{D-1}\sum_{\alpha=1}^{D} c_k^\alpha$$

$$\sum_{ij} = \frac{1}{D-1}\sum_{\alpha=1}^{D} (c_i^\alpha - \overline{c}_i)(c_j^\alpha - \overline{c}_j)$$

Matrix U_{ki} is the rotation matrix, which diagonalizes the dispersion matrix Σ_{ij}, and with the help of U_{ij} one can obtain the function F_i for the filter :

$$\sum_j \sum_{ij} U_{jk} = \lambda U_{ik}, \; F_i \sum_k \psi_k U_{ik}$$

Figures 16 and 17 illustrate the filters $F_i(x,z)$ for the first four main components in the D1 representation and two components for D2 (Daubechies1,2) images. From the Figures it is seen that the filter F_1 of the D1 image and the linear combination of the filters F_1 and F_2 of the D2 image are responsible mainly for the motion of gases from top to bottom (in the direction of acceleration g). Note that F_2-F_1 is similar to the function F_1 for D1. The rest of the filters (the filters of i≤17 and i≤40 were analyzed) are responsible, mainly, for the description of the liquid overflowing in the x-direction, where the greater the "i" the lesser the scale of the overflowing. The SMC corresponds to the absence of liquid overflowing in the x-direction. Figure 18 demonstrates the dependence of the first main components on time $(PC)_1^j$ together with the zone width and the mass in the mixing zone. Figure 18 for the time dependence $(PC)_1^j$ demonstrates a proximity of the notions "zone width", "intruded mass", and "the first main component".

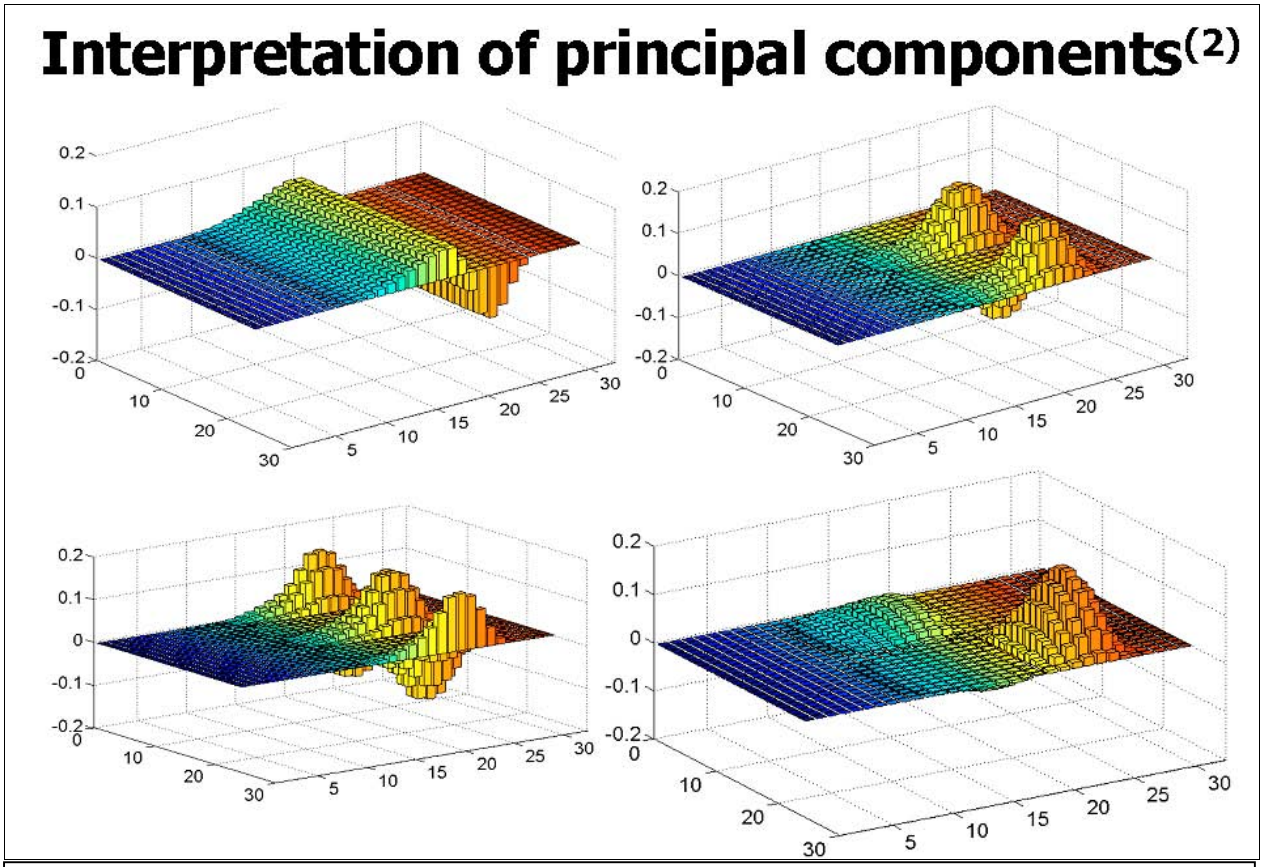

Fig. 16. Filter $F_i(x,z)$ for the first four main components Daubechies 1

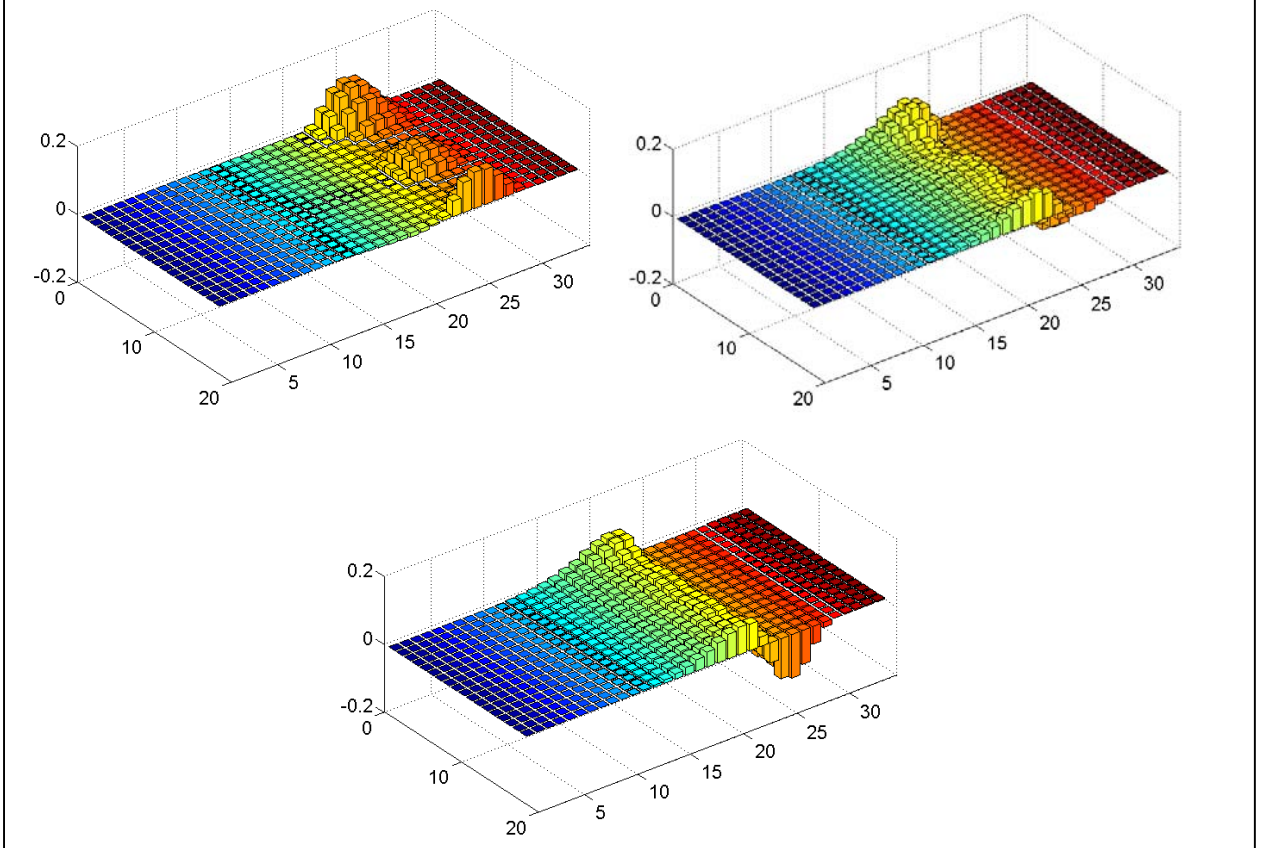

Fig. 17. Filter $F_i(x,z)$ for main components 1 and 2 - Daubechies 2 (D2) and their linear combination F_2 - F_1

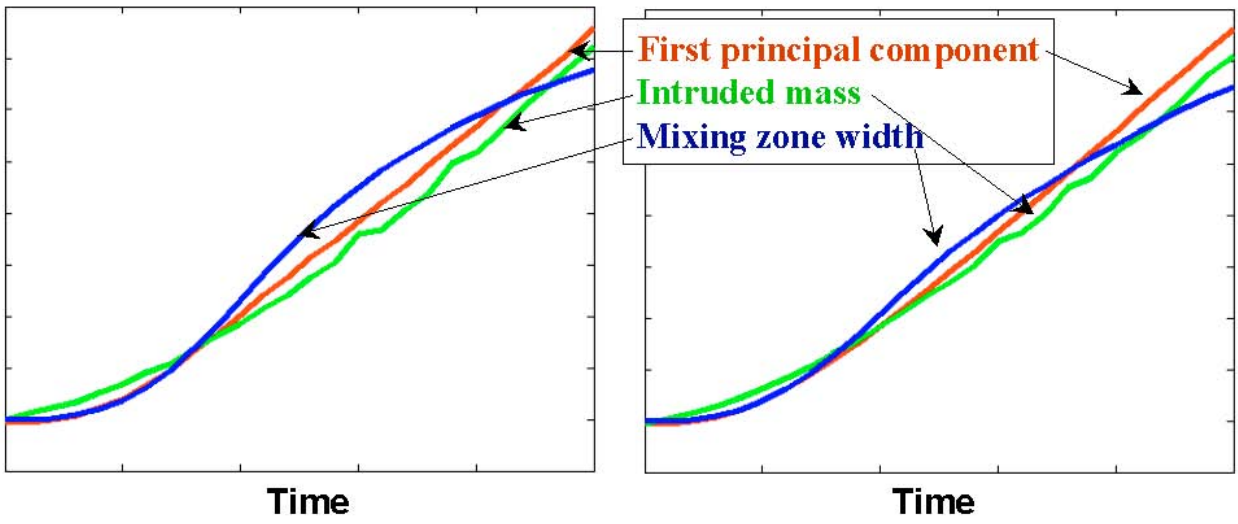

Fig. 18. The first main component evolution in time : at the right – for one of the calculations, at the right – for average by all the calculations.

It seems interesting and perspective to study henceforth the interpretation of the main components.

It proves possible to predict finite results by the primary data thanks to the ability of the Kohonen map to distinguish “far” and “close” (similar and non-similar) calculations. This question is considered in more detail in a separate paper [9].

If the initial data are so that a simulation starts at a certain point of the Kohonen map (in a cluster), it might be probably found, as a result of evolution, in the next clusters, and finally in several clusters within a certain area of the Kohonen map. On this basis, Fig. 19 illustrates the predicted turbulent mixing.

4. Conclusion

Numerous 2D and 3D simulations of RT and RM instabilities and turbulent mixing were performed for different initial conditions of the initial perturbation mode compositions, amplitudes, the gases participating in the mixing process, and different statistical realizations of equitype simulations. The DNS data, their processing, and the derived dependencies allow one to answer an important, e.g. for the LTF, question about the dependence of the mixing characteristics (at the thermonuclear target compression) on the initial conditions. Note the found weak dependence of the mixing zone width on the deposition from the high modes (a large deposition from the high modes slightly reduces the mixing zone width). The zone widths for 2D and 3D problems turn to be close for the close initial conditions. An analytical formula for the mixing zone width $L(t)$, which satisfactorily describes the results for a wide range of the initial conditions, was derived.

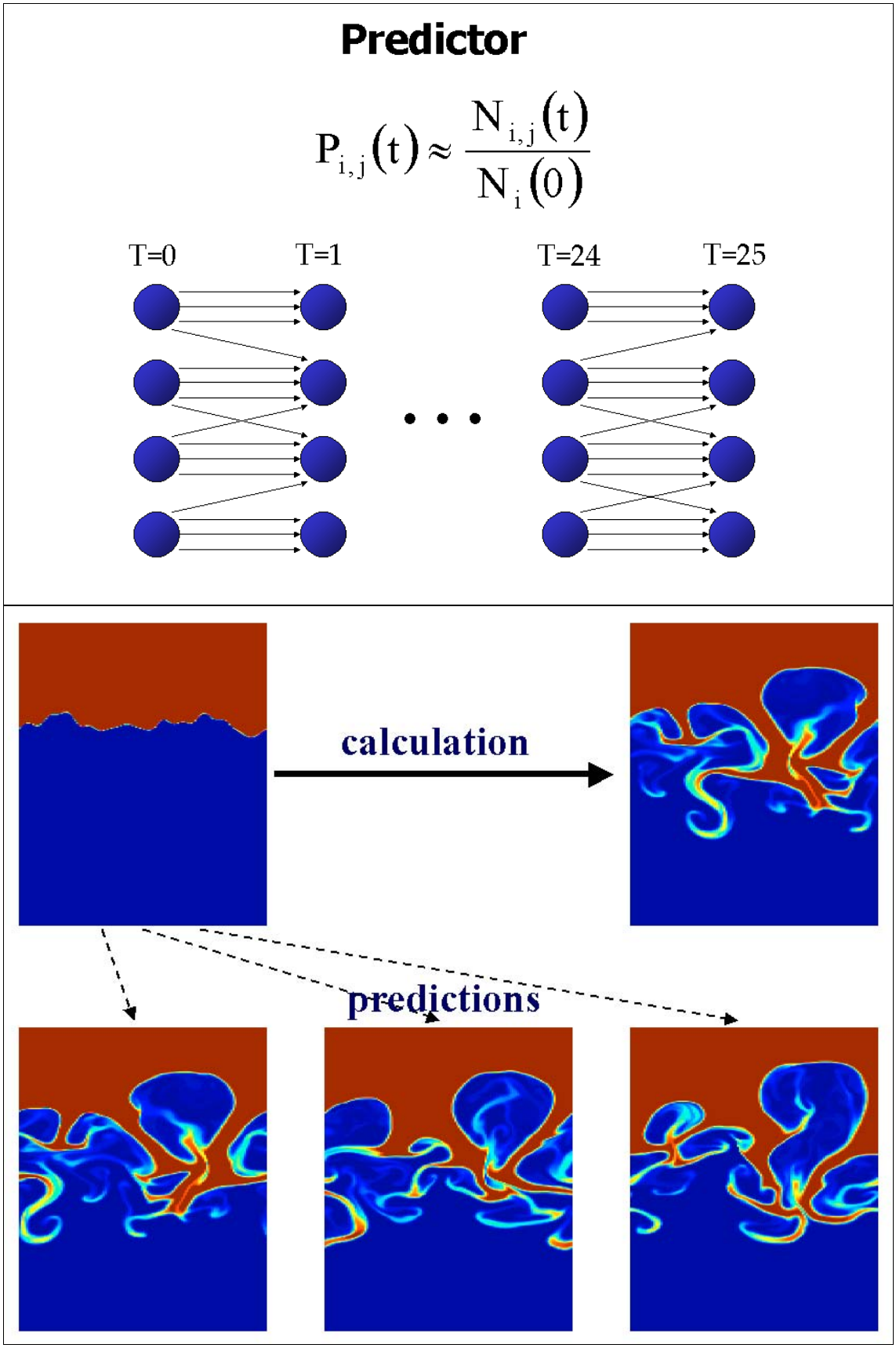

Fig. 19. The instability development prognosis. At the top – arrows shows the simulation probable development path. At the bottom are presented 3 possible variants, chosen on the base of the initial conditions information

A wavelet analysis of the DNS data was performed. It was shown that the wavelet representation is stable and recognizes well the simulations with different physical characteristics. The best properties have the wavelets with the lower-order dimensionality D1 (Haar or Daubechies). The used technique of 2D Kohonen maps allowed one to find the similarity of the processes close by their physical parameters.

The interpretation of the main components of wavelet space after its compression and reducing of dimensionality from ~ $3 \cdot 10^4$ to several tens or hundreds seems to be an interesting and promising problem. The obtained filters (in some sense, the eigen-functions of the problem) contain the data on the gas motion, and it is interesting to present these data in the form of fields of physical values. In the representation D1 the first main component is comparable to such physical quantities as time, mixing zone width, "intruded" mass.

Basing on the developed representations, we proposed and realized an example of a neuron net, which, after being learnt on a certain sampling of simulations, is able to predict the final state of the mixed gases using the initial perturbation data.

The work was supported by the ISTC within the framework of the Project#1481. The authors are grateful to David Youngs (AWE, UK) and Stuart Dalziel (Batchelor Laboratory, University of Cambridge, UK) for fruitful discussions and comments, and to I.Doskoch for the help in preparation of the article and its electron version.

References

1. A.N.Aleshin, E.V.Lazareva, E.I.Chebotareva, S.V.Sergeev, S.G.Zaytsev. "Investigation of Richtmyer-Meshkov instability induced by the incident and the reflected shock waves". Proc. of the Sixth International on the Physics of Compressible Turbulent Mixing, Marseille, 1997, pp.1-6.
2. V.F.Tishkin, V.V.Nikishin, I.V.Popov, A.P.Favorsky. "Difference scheme of three-dimensional gas dynamics for the solution of Richtmyer-Meshkov instability problems". Mathematical modeling 7(5), 15, 1995.
3. N.N.Anuchina, V.I.Volkov, N.S.Es'kov. "Numerical method of calculation of the contact boundaries with large deformations". International conference "Zababakhin's Readings" Snezhinsk, 1998.
4. N.N. Anuchina, V.I. Volkov, V.A.Gordichuk, N.S. Es'kov, O.S.Ilyutina, O.M.Kozyrev. "The method and MAX-3 program complex for a numerical simulation of 3D gas dynamic problems". Abstracts of reports of XII All-Russia Conference "Theoretical grounds and designing of numerical algorithms of mathematical physics problems", Novorossiisk, 1998.
5. N.N. Anuchina, V.I. Volkov, N.S. Es'kov. " A method for numerical simulation of contact surface with high distortions ". In: Proceedings of the 7th IWPCTM (St. Petersburg, Russia, July 1999).
6. Yu.V. Yanilkin. "Numerical modeling of 2D flows with account for certain small-scale processes". Physical mesomechanics, v.2, №5, pp.27-48, 1999.
7. N.V. Zmitrenko, N.G. Proncheva, V.B. Rozanov. "Evolutionary model of the turbulent mixing layer". Preprint FIAN № 65, 1997.

8. D. Layzer “Astrophysical Journal On the stability of superpose fluids in an gravitational field ”, v. 122, №1, p.1-12, 1995.
9. A.S. Nuzhny V.B. Rozanov, R.V. Stepanov, S.A. Shumsky “Studying of Rayleigh-Taylor instability in the ICF problem by the methods of linear statistics”. Preprint FIAN № 32, 2002.
10. A.S. Nuzhny, V.B. Rozanov, R.V. Stepanov, S.A. Shumsky “Study of Rayleigh-Taylor instability in inertial laser fusion problem and comparison of different calculation methods by wavelet coding of the initial physical fields and their neuronet processing ”. Preprint of P.N. Lebedev Physical Institute of Russia № 12, 2004.
11. I. Daubechies “ Ten lectures on Wavelets ”. CBMS-NSF Regional Conf. Series in Appl. Math., Vol. 61. Society for Industrial and Applied Mathematics, Philadelphia, 1992.
12. A.A. Ezhov, S.A. Shumsky “Neurocomputing and its application to economics and business”. Moscow, MEPHI, 1998.
13. T. Kohonen “Self-Organized formation of topologically correct feature maps”. Biol. Cybernetics 43, 56-59.